Endothelial AGGF1 promotes retinal angiogenesis by coordinating TNFSF12/FN14 signalling

Ying Cheng [1,3], Man Zhang [1,3], Chenguang Li[1], Long Su[1,2], Lingli Fu[1], Shi Wu[1], Chaofei Xu[1], Bei Sun [1] ✉ & Liming Chen [1] ✉

Abnormal angiogenesis is a key process associated with ischaemic retinopathies such as diabetic retinopathy, for which the underlying pathological mechanisms are still poorly understood. Here, we confirm that angiogenic factor 1 with a G patch and FHA domain (AGGF1) is elevated in the diabetics and induces retinal angiogenesis. Mechanistic investigations demonstrate that HIF-1α directly regulates *AGGF1* expression. AGGF1 upregulates the expression of cell cycle proteins by increasing the binding of tumour necrosis factor ligand superfamily member 12 (TNFSF12) to fibroblast -growth -factor-inducible 14 (FN14, TNFRSF12A). Furthermore, targeting AGGF1 attenuates pathological neovascularisation in ischaemic retinopathy. Additionally, we discover that sodium-glucose cotransporter 2 inhibitors (SGLT2i) could inhibit the AGGF1 signalling pathway early to achieve therapeutic effects. Overall, we elucidate the mechanism underlying pathological retinal angiogenesis involved in endothelial AGGF1-dependent events and highlight a therapy for the effective treatment of ischaemic retinopathy.

Ischaemic retinopathy, which includes diabetic retinopathy (DR)[1–4], retinopathy of prematurity (ROP)[5–7], and age-related macular degeneration (AMD)[8–10], is the leading cause of blindness in industrialised countries[11]. It is characterised by disorganised and leaky neovascularisation[4,6,7,12]. Therefore, pathological angiogenesis has been established as a key target for the treatment of these retinal vascular diseases[13,14]. Vascular endothelial growth factor (VEGF), an angiogenic factor, is a critical regulator of angiogenesis[15]. Intravitreal injection of anti-VEGF drugs have been successfully used in clinical studies[16,17]. However, VEGF neutralisation therapy carries a major risk of accelerating the atrophy of photoreceptors in certain patients[18,19] and is ineffective in some patients with vascular diseases[20]. Consequently, there is an urgent need to identify novel therapeutic targets.

AGGF1, also known as VG5Q, is a novel angiogenic factor that plays a key role in angiogenesis and vascular development[21–24]. This molecule was the first susceptibility gene identified in the rare inherited vascular disease Klippel Trenaunay syndrome (KTS), in which genetic mutations lead to KTS[21,25]. KTS is primarily characterised by varicose veins and capillary malformations[26], and its pathogenesis is associated with excessive angiogenesis and AGGF1 expression[21]. Previous studies have shown that AGGF1 is highly expressed in endothelial cells and exhibits functions similar to those of VEGF, which can promote endothelial cell proliferation, migration, and angiogenesis[25]. Moreover, AGGF1 was reported to be highly expressed in tumour tissues of gastric, hepatocellular and colorectal cancers and could regulate tumour angiogenesis[27,28]. However, the role of AGGF1 in ischaemic retinopathy remains unclear.

In this study, we used genetic and pharmacological blocking assays to investigate the function of AGGF1 and the underlying mechanisms of retinal pathological angiogenesis. We discovered that the elevation of AGGF1 is a major biological process that causes retinal angiogenesis. We also provided evidence that EC-specific

[1]NHC Key Lab of Hormones and Development and Tianjin Key Lab of Metabolic Diseases, Tianjin Medical University Chu Hsien-I Memorial Hospital & Institute of Endocrinology, Tianjin, China. [2]The Second Hospital of Tianjin Medical University, Tianjin, China. [3]These authors contributed equally: Ying Cheng, Man Zhang. ✉e-mail: sun_peipei220@hotmail.com; xfx22081@vip.163.com

AGGF1 knockout ameliorates pathological angiogenesis and vaso-obliteration in oxygen-induced retinopathy (OIR) retinas. Furthermore, we demonstrated that AGGF1 increases the binding of tumour necrosis factor ligand superfamily member 12 (TNFSF12) to fibroblast -growth -factor-inducible 14 (FN14, TNFRSF12A) and promotes pathological retinal angiogenesis by upregulating cell cycle proteins. Additionally, we discovered that sodium-glucose cotransporter 2 inhibitors (SGLT2i) inhibit the AGGF1 signalling pathway early and thus delay retinal disease progression. We elucidated the mechanism of action of AGGF1 in the pathological process of retinal angiogenesis and identified it as a potential therapeutic target for the treatment of retinal pathological neovascularisation. Our study proposes a therapeutic target for ischaemic retinopathy.

Results

AGGF1 was upregulated in the retinas of db/db mice and was also increased in the vitreous fluid of patients with proliferative diabetic retinopathy

To observe morphological changes in the retinas of db/db mice, we first assessed retinal thickness in db/db mice using a noninvasive optical coherence tomography (OCT) in vivo and HE staining (Supplementary Fig. 1a–c). Retinal thickness was significantly reduced in db/db mice compared to age-matched db/m mice. Retinal trypsin digestion assays showed that the number of acellular capillaries was markedly increased in db/db mice (Supplementary Fig. 1d, e). To further understand these roles, we performed a proteomic analysis of db/m and db/db mouse retinas. Unexpectedly, the expression of the angiogenic factor AGGF1 was significantly elevated in db/db mice (Fig. 1a and Supplementary Fig. 2a and Supplementary Data 1). Western blot analysis and immunohistochemical staining further confirmed a significant increase in AGGF1 protein levels in db/db retinas compared to retinas from db/m mice (Fig. 1b–d).

AGGF1 functions as an angiogenic factor and is, therefore, a key target in angiogenesis[21]. We found that AGGF1 expression increased in the retinas of db/db mice, which was not supported by the histology associated with this model, as angiogenesis is not typically associated with db/db mice. However, the presence of ischaemia and hypoxia in the retinas of db/db mice was likely why AGGF1 expression was increased in db/db mice. To identify the effect of AGGF1 in clinical ischaemic retinopathy, we evaluated the concentration of AGGF1 in the vitreous fluid of patients with proliferative diabetic retinopathy (PDR). The severity of injury in patients with PDR was first evaluated using fundus fluorescein angiography (FFA) and OCT (Fig. 1e). Patients with nonvascular retinopathies were used as controls (Supplementary Table 1). We found that the overall retinal and ganglion cell layer thicknesses were significantly reduced (Supplementary Fig. 3a). Western blotting revealed a significant increase in AGGF1 levels in the vitreous fluid of patients with PDR (Fig. 1f, h). The representative proangiogenic factor, VEGF, was also elevated in the PDR group (Fig. 1g, h). We also collected data on the aqueous humours of patients with diabetic patients, non-proliferative diabetic retinopathy (NPDR) and PDR. The protein levels of AGGF1 and VEGF were higher compared with controls, but lower to NPDR and PDR (Fig. 1i–m), suggested that the expression of AGGF1 was gradually increased during progression of non-diabetes to diabetes to diabetic retinopathy. This further explains why AGGF1 expression was elevated in the retinas of db/db mice. Research has shown that persistent hyperglycaemia damages the retinal vasculature[29], leading to retinal ischaemia and the secretion of angiogenic factors that promote neovascularisation[30]. Collectively, these data provide a rational context for exploring the role of AGGF1 in clinical ischaemic retinopathy.

AGGF1 was upregulated in retinas with oxygen-induced retinopathy and colocalized with neovascular endothelial cells

Angiogenic factors play distinct roles in vascular disease development. To determine whether AGGF1 plays an important role in pathological angiogenesis, we investigated retinal AGGF1 levels at different phases in an oxygen-induced retinopathy (OIR) mouse model (Fig. 2a), which has been widely used to simulate the pathological process of human PDR and retinopathy of prematurity (ROP)[31]. In the OIR model, newborn mice were first exposed to 75% oxygen from postnatal day 7 (P7) to P12, which lead to vaso-obliteration in the centre of their retinas. After the animals were returned to room air, the abnormal neovascularisation gradually proliferated, from P12 to P17. Subsequently, the abnormal vessels regressed from P17 to P21 (Fig. 2b and Supplementary Fig. 4a). Western blot analysis revealed that AGGF1 did not change in the retinas of normoxic mice from P12 to P21 (Supplementary Fig. 5a, b); however, it consistently increased during the neovascularisation stage of OIR compared to the vessel regression stage of OIR, which was consistent with VEGF protein levels in the OIR model (Fig. 2c, d). In addition, compared to that in the normoxic mouse retinas, AGGF1 increased in the P17 OIR mouse retinas (Supplementary Fig. 6b, c). Overall, these data illustrate that the dynamic expression of AGGF1 is relevant in clinical proliferative retinopathies, especially in the neovascularisation phase. To explore the spatiotemporal expression of AGGF1 in pathological retinal neovascularisation, we compared the AGGF1 expression in the P12, P17, and P21 OIR mouse retinas. We found that the expression of AGGF1 gradually increased from P12 to P17, regressed from P17 to P21, and was markedly expressed in each vascular plexus (superficial, intermediate, and deep vascular plexuses) of the P17 OIR group mouse retinas (Fig. 2e, f). In addition, AGGF1 increased in the P17 OIR mouse retinas and was distinctively colocalized with CD31 in the P17 OIR mouse retinal sections, as shown by immunofluorescence staining (Fig. 2g). Consistent with the previous results, endogenous AGGF1 expression was verified by immunostaining of whole-mount retinas (Fig. 2h). Moreover, immunostaining of whole-mount retinas revealed that AGGF1 was expressed in both macrovascular and microvascular vessels in the retinas of the mice in the P17 OIR group (Fig. 2i, j); however, AGGF1 was barely colocalized in the astrocytes or microglia (Fig. 2k). These results further demonstrate that the upregulated AGGF1 protein is derived from retinal endothelial cells (EC) during the pathological angiogenesis phase.

Endothelial AGGF1 deficiency significantly ameliorated retinal pathological angiogenesis and vaso-occlusion in OIR mice

To further reveal the function of AGGF1 in retinal pathological neovascularisation, we constructed endothelial cell *Aggf1*-specific knockout mice (Supplementary Fig. 6a) and tested their knockout efficiency (Supplementary Fig. 6b–e). We tested OIR retinas from *Aggf1* knockout mice at different time points ranging from P12 to P21. When exposed to normoxia, endothelial *Aggf1* deletion had no impact on the physiological processes of vessel development (Fig. 3a–c). Additionally, we found no obvious difference in avascular and neovascular tufts (NVTs) areas between the *Cdh5-Cre Aggf1*^fl/fl^ and *Aggf1*^fl/fl^ mice at the beginning of angiogenesis (Fig. 3d, g) or at the regression stage of OIR (Fig. 3f, i). However, compared to the Aggf1^fl/fl^ mice, the avascular and NVTs areas were significantly decreased in the *Cdh5-Cre Aggf1*^fl/fl^ mice at P17 (Fig. 3e, h and Supplementary Fig. 7a) during the pathological neovascularisation stage of OIR. These findings indicated that endothelial *Aggf1* deficiency simultaneously promoted normal vascular growth in the ischaemic retina and abnormal vascular regression in OIR mice. Previous studies have shown that the leakage of vascular and inflammatory cells is the underlying cause of exacerbating retinal vasculopathy[32]. We found that TER119-positive red blood cells (RBC) leakage in the *Cdh5-Cre Aggf1*^fl/fl^ OIR mice was lower than that in the *Aggf1*^fl/fl^ OIR mice at P17 (Fig. 3j), suggesting that the vasculature of the
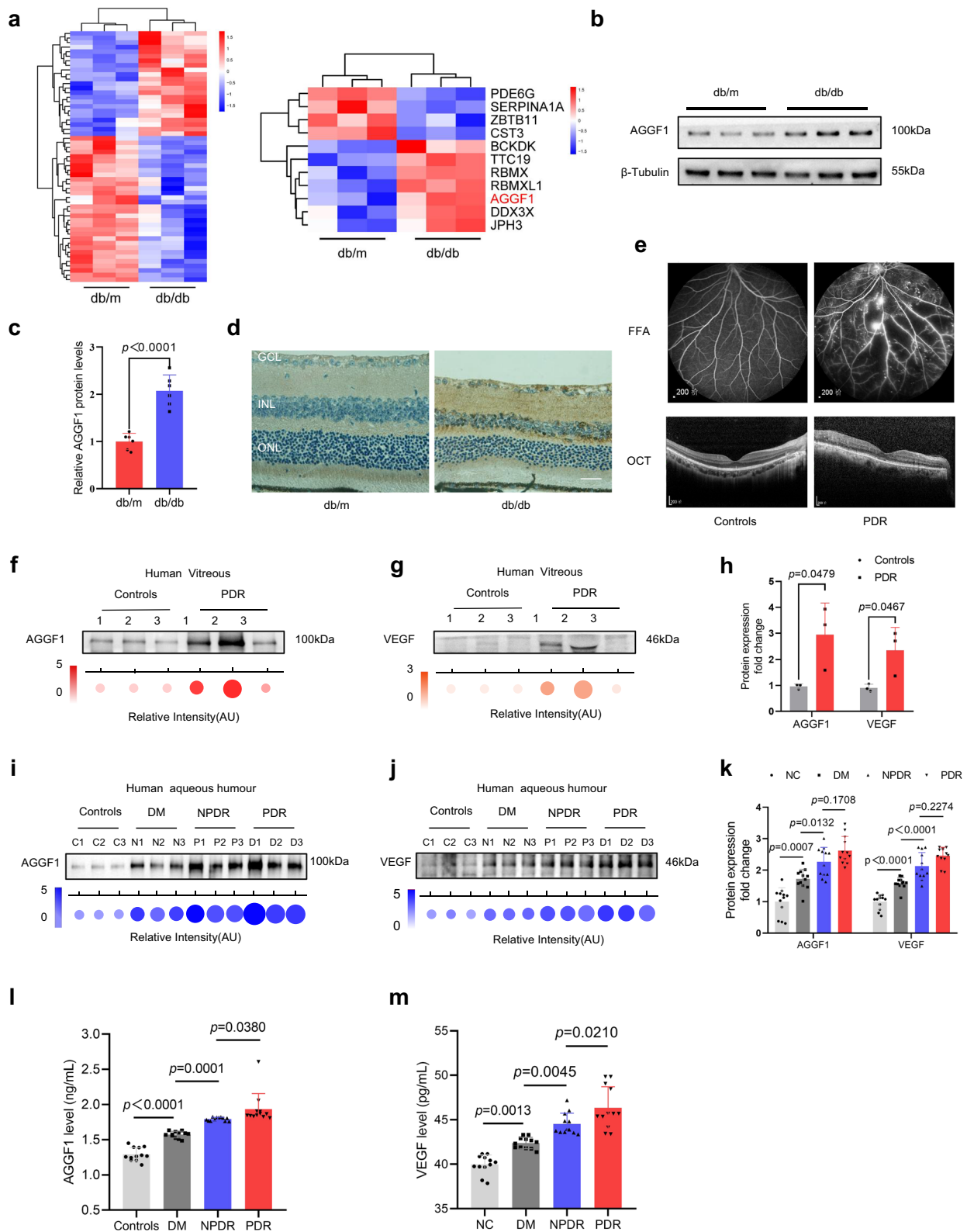
Fig. 1 | AGGF1 is elevated in the retinas of db/db mice and in the vitreous of patients suffering from PDR. a Heat maps from proteomic array analysis with ranked enriched genes in 3 db/m retina compared with 3 db/db retina (fold-change >1.2 or <0.83, $p < 0.05$). High and low expression are denoted by red and navy, respectively. **b, c** Western blot analysis and quantification of AGGF1 protein levels in db/m retina and db/db retina ($n = 6$ mice per group). **d** Immunohistochemical detection of AGGF1 expression in db/m and db/db mice. Scale bar: 50 µm. **e** Representative fundus fluorescein angiography (FFA) and SD-OCT pictures obtained from patients with PDR. $n = 3$ individuals. Scale bars: 2000 µm (top),

500 µm (centre). **f–h** Western blot analysis and quantification of AGGF1 and VEGF protein levels in equal volumes of vitreous fluid from patients. $n = 3$ individuals. **i–k** Western blot analysis and quantification of AGGF1 and VEGF protein levels in equal volumes of aqueous humour from patients. $n = 12$ individuals. **l, m** The ELISA analysis of AGGF1 and VEGF levels in aqueous humour from patients. $n = 12$ individuals. Error bars represent mean ± SEM. 2-tailed unpaired Student's t test (**a, c, h**) and one-way ANOVA with Tukey's multiple comparisons test (**k, l, m**). GCL ganglion cell layer, INL inner nuclear layer, ONL outer nuclear layer. Source data are provided as a Source Data file.
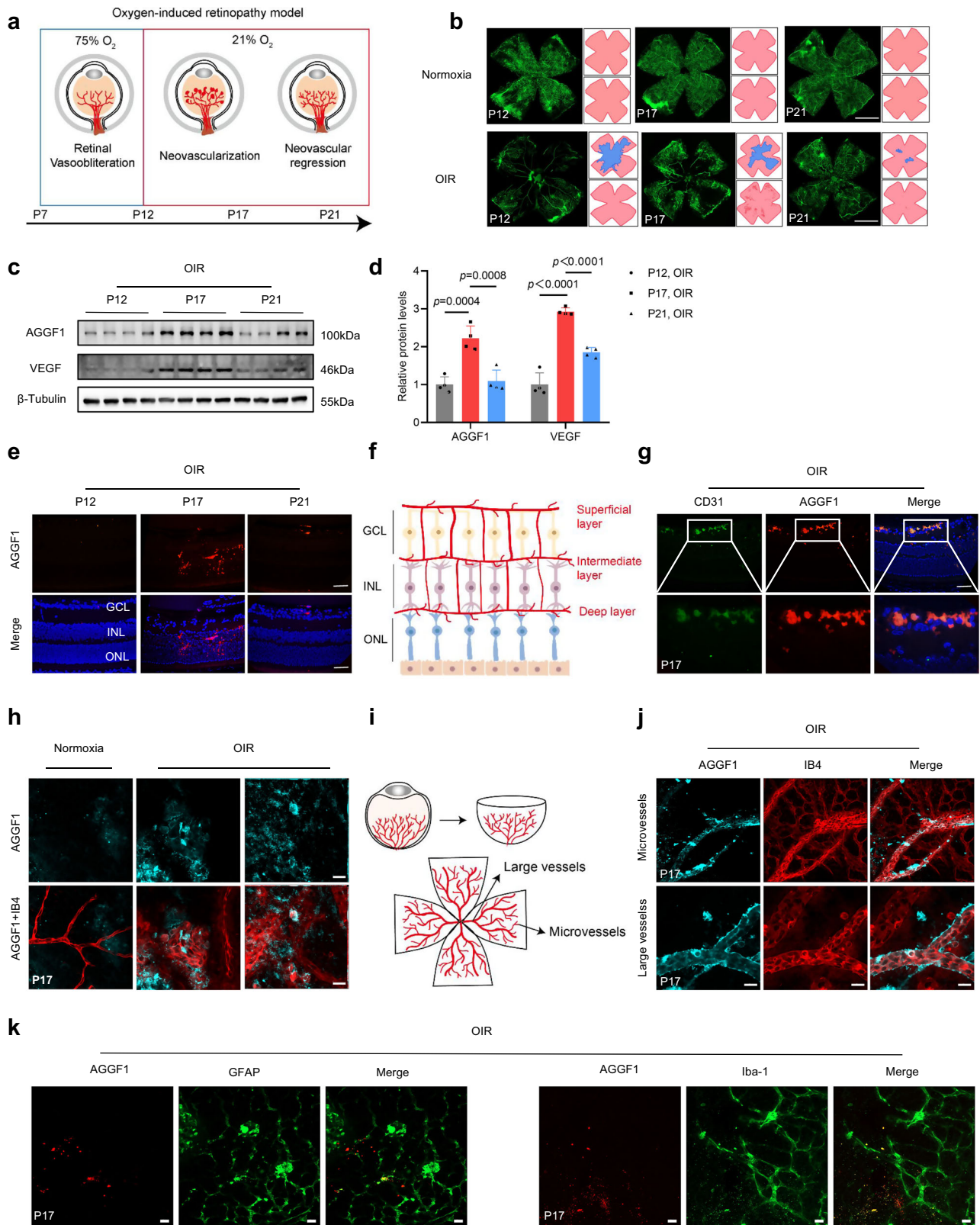
Cdh5-Cre Aggf1^fl/fl OIR retinas was more mature and not leaky. Moreover, the F4/80-positive macrophages in the *Cdh5-Cre Aggf1^fl/fl* OIR mice were lower than that in the *Aggf1^fl/fl* OIR mice at P17 (Fig. 3k). Thus, our study revealed that endogenous AGGF1 depletion prevented worsening of vascular diseases in OIR mouse retinas.

Next, we investigated the mechanism by which endogenous AGGF1 promoted vascular disease in OIR mouse retinas. It is already

known that insufficient perfusion causes retinal hypoxia and the release of large growth factors, leading vasculopathy in PDR[33,34]. Given that AGGF1 expression was increased both in the OIR mouse retinas and in the eyes of patients with PDR, we tested whether hypoxia upregulated the expression of AGGF1 in human retinal microvascular endothelial cells (HRMECs). Western blotting revealed that the protein levels of AGGF1 were significantly upregulated in

Fig. 2 | AGGF1 is elevated in the retinas of the OIR mice and co-localized with neovascular endothelial cells. a Schematic illustration of the mouse oxygen-induced retinopathy (OIR) model. **b** FITC-dextran staining of whole-mount retinas from normoxic and OIR mice at P12, P17, and P21 (*n* = 3 mice per group). In the inserts, the red line represents the edge of the retina, the blue area represents the avascular area, and the red area represents neovascular tufts (NVTs). **c, d** Western blot analysis and quantification of AGGF1 and VEGF protein levels in the OIR retinas at P12, P17, P21 (*n* = 4 mice per group). **e** Immunofluorescence staining for AGGF1 on retinal sections at P12, P17, and P21 of OIR mice (*n* = 4 mice per group). AGGF1 is expressed by blood vessels in the superficial, intermediate, and deep layers. **f** Schematic illustration of the structure of retinal layers and the distribution of vessels in retinal sections. **g** Double immunofluorescence staining for AGGF1 (red) and CD31 (green) in P17 OIR retinas (*n* = 4 mice per group). **h** Localization and quantification of AGGF1 protein in whole-mount retinas upon normoxia and OIR at P17 (*n* = 5 mice per group). **i** Schematic illustration of the vascular network in flat-mounted retinas. **j** Immunofluorescence for AGGF1 and isolectin B4 (IB4) in whole-mounted retinas of OIR mice at P17 (*n* = 5 mice per group). AGGF1 co-localized with IB4 in microvessels and large blood vessels. **k** Immunofluorescence for AGGF1 and Iba-1 (a microglial marker) and GFAP (an astroglial marker) in whole-mount retinas of OIR mice at P17 (*n* = 5 mice per group). Error bars represent mean ± SEM. One-way ANOVA with Tukey's multiple comparisons test (**d**). Scale bars: 1000 μm (**b**), 50 μm (**e, g**) and 100 μm (**h, j, k**); magnified images: 50 μm (**g**). GCL ganglion cell layer, INL inner nuclear layer, ONL outer nuclear layer. Source data are provided as a Source Data file.

HRMECs after being exposed to high glucose (HG) (Supplementary Fig. 9a).

Hypoxia-inducible factors (HIFs) regulate gene expression under hypoxic conditions[35]. We found that HIF-1α was elevated in HRMECs exposed to HG (Supplementary Fig. 8a, b). Interestingly, the increase of AGGF1 correlated with the HIF-1α levels. To investigate the role of HIF-1α in regulating AGGF1 expression, we performed HIF loss-of-function studies. Western Blot showed that knockdown of *HIF-1α* significantly downregulated AGGF1 expression under HG exposure (Supplementary Fig. 8c–g). We next analysed the sequence characteristics of the *AGGF1* promoter and identified *HIF-1α* that directly binds to the *AGGF1* promoter. Using the JASPAR database (https://jaspar2022.genereg.net/ JASPAR - A database of transcription factor binding profiles (genereg.net)), we identified that HIF-1α directly binds to the AGGF1 promoter and activates its transcription upon hypoxia (Supplementary Fig. 8h). Thus, these data suggest that the expression of endothelial AGGF1 is regulated in a HIF-1α−dependent manner upon HG exposure.

AGGF1 promoted angiogenesis by upregulating proliferation-related indicators

Next, we investigated the mechanism by which endogenous *Aggf1* deficiency attenuated retinal vasculopathy in OIR mice. In the early stages of diabetic retinopathy (DR), microvascular dysfunction, loss of the retinal blood supply, and impaired nutrient and oxygen delivery occur. Subsequently, in PDR, tissue ischaemia and hypoxia trigger the release of angiogenic and inflammatory mediators that promote vasculopathy[36]. Given that AGGF1 protein levels were increased in the retinas of db/db and OIR mice, and in the vitreous fluid of patients with PDR, we examined whether HG levels increased the levels of AGGF1 in ECs. Western blot analysis revealed that the expression of AGGF1 was markedly upregulated in HG-treated HRMECs (Supplementary Fig. 9a). To better understand the intracellular molecular mechanisms by which AGGF1 modulates angiogenesis, we silenced endogenous AGGF1 expression in HRMECs using *AGGF1*-specific small interfering RNA (siRNA) to reduce AGGF1 protein levels (Supplementary Fig. 9a). Heatmaps and volcano plot from the proteomic array analysis listed the upregulated and downregulated genes between the control and the *AGGF1*-silenced HRMECs (Fig. 4a and Supplementary Fig. 10a and Supplementary Data 2). Gene Ontology (GO) terms showed that the differentially expressed genes (DEGs) were mainly enriched in the cell cycle (Fig. 4b and Supplementary Data 2). Kyoto Encyclopedia of Genes and Genomes (KEGG) pathway analysis showed that the DEGs were primarily enriched in the cell cycle of *AGGF1*-silenced HRMECs compared to controls (Fig. 4c and Supplementary Data 2). Proliferation and migration of endothelial cells are required for angiogenesis to occur[37]. Vascular endothelial cells are activated by hyperglycaemia, which accelerates vascular disease[38,39]. Therefore, AGGF1 may regulate cell-cycle progression. We observed a significant reduction in the levels of the cell cycle proteins CyclinA2, CyclinD1, and CDK1 in *AGGF1*-silenced HRMECs exposed to HG levels (Fig. 4d, e). Moreover, cell proliferation, migration and tube-forming ability were significantly reduced in *AGGF1*-silenced HRMECs compared to controls exposed to HG levels (Fig. 4f–i), which is consistent with the above notion. These data indicated that *AGGF1* knockdown reduced pathological angiogenesis by decreasing cell proliferation in the context of hyperglycaemia. To provide further evidence that cell cycle proteins are the downstream regulators of AGGF1 during pathological angiogenesis, we overexpressed endogenous AGGF1 in HRMECs using an *AGGF1*-specific plasmid. However, AGGF1 overexpression barely upregulated the expression of the cell cycle proteins CyclinA2, CyclinD1 and CDK1 (Supplementary Fig. 11a, b); therefore, we evaluated whether AGGF1 interacted with other proteins to promote angiogenesis.

AGGF1 promoted the binding of TNFSF12 to Fn14 to increase angiogenesis

AGGF1 (V5GQ) is known to promote angiogenesis by interacting with TNFSF12 (TWEAK)[21]. TNFSF12, is a member of the tumour-necrosis factor (TNF) superfamily that induces angiogenesis in vivo[40]. In the present study, we used the STRING website (STRING: functional protein association networks (string-db.org)) to identify interactions between AGGF1 and TNFSF12 (Fig. 5a). By performing co-immunoprecipitation (Co-IP) assays, we were able to validate that AGGF1 binds to TNFSF12 with high affinity (Fig. 5b). Notably, western blot analysis revealed that the expression of TNFSF12 was markedly upregulated in HG-treated HRMECs (Supplementary Fig. 12a, b), and that TNFSF12 was continuously elevated during the neovascularisation stage of OIR compared with the vessel regression stage of OIR (Supplementary Fig. 12c, d). To better understand the intracellular molecular mechanisms by which TNFSF12 modulates angiogenesis, we silenced endogenous TNFSF12 expression in HRMECs using *TNFSF12*-specific small interfering RNA (siRNA) to reduce TNFSF12 protein levels (Supplementary Fig. 13a, b). The results revealed a significant reduction in the cell cycle proteins CyclinA2, CyclinD1, and CDK1 in *TNFSF12* KO HRMECs exposed to HG (Fig. 5c, d). Moreover, cell proliferation and migration were significantly reduced in *TNFSF12*-silenced HRMECs compared to controls (Fig. 5e–g). However, expression of the cell cycle proteins CyclinA2, CyclinD1, and CDK1 were barely upregulated when TNFSF12 was overexpressed (Fig. 5h and Supplementary Fig. 14a). We further observed that cell cycle proteins were distinctively increased in *AGGF1* + *TNFSF12*-overexpressing HRMECs compared to those in blank controls (Fig. 5i and Supplementary Fig. 15a). Moreover, cell proliferation was significantly increased in *AGGF1* + *TNFSF12*-overexpressing HRMECs compared to that in blank controls (Fig. 5j). Previous studies have shown that the fibroblast growth factor-inducible 14 (Fn14) receptor binds to TNFSF12, forming a homo-trimer to promote angiogenesis[40]. The STRING website reports an interaction between TNFSF12 and TNFRSF12A (FN14) (Fig. 5k). In our study, Co-IP showed that FN14 strongly interacted with TNFSF12 but not with AGGF1 (Fig. 5l). However, we found that it had no influence on the expression of TNFSF12 either in vivo *or* in vitro when *AGGF1* was knocked down (Supplementary Fig. 16a–d). This suggests that AGGF1 may influence the binding of TNFSF12 to FN14 to mediate downstream signal transduction. Our results revealed that the binding of TNFSF12
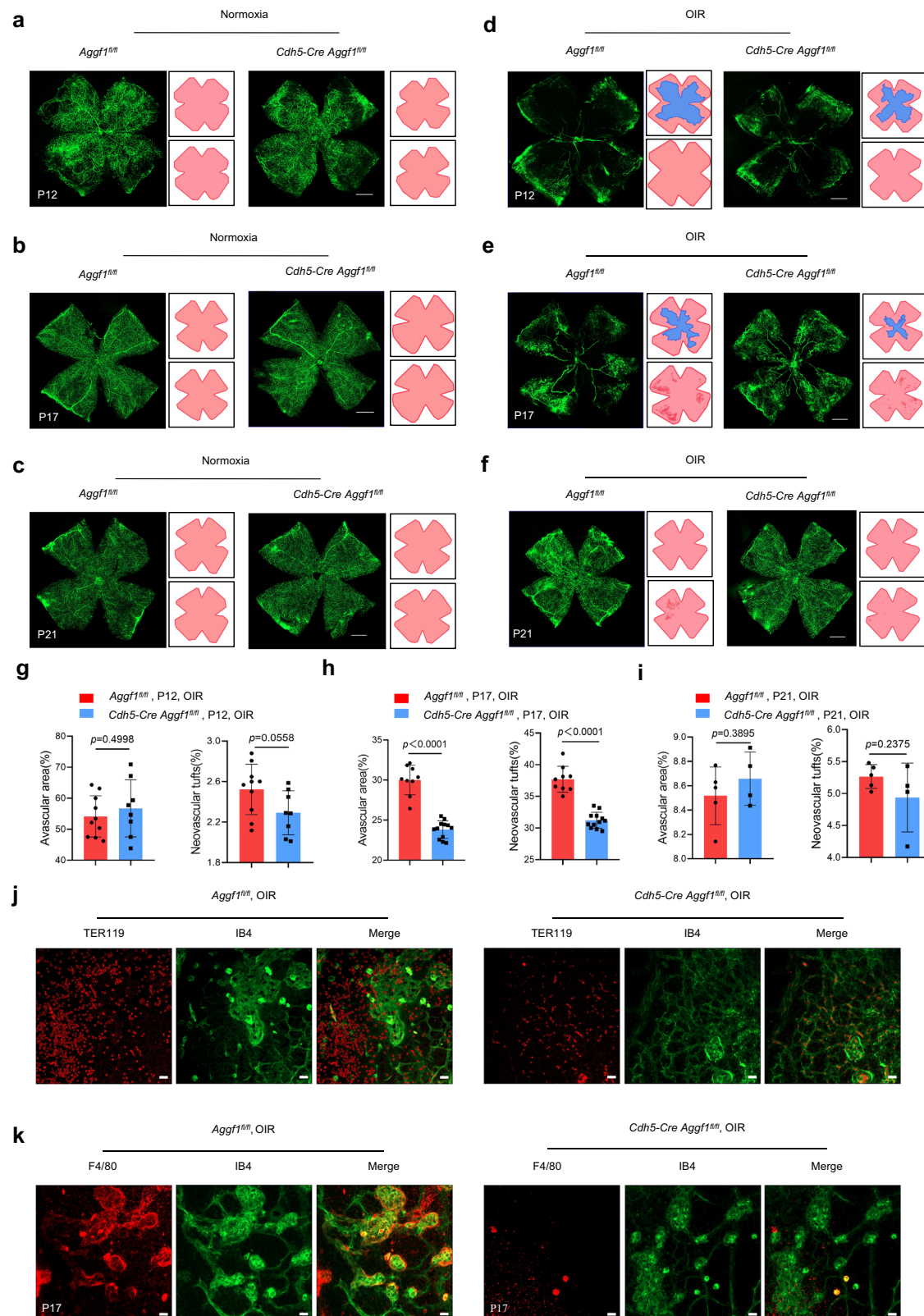
Fig. 3 | Endothelial AGGF1 deficiency significantly ameliorated pathological neovascularisation in the OIR model. a–i FITC-dextran staining of whole-mount retinas and quantification of the avascular area and NVTs area from *Aggf1*^fl/fl^ and *Cdh5-Cre Aggf1*^fl/fl^ normoxic and OIR mice at P12 (**a**, **d**, **g**) (*n* = 10 *Aggf1*^fl/fl^ and 8 *Cdh5-Cre Aggf1*^fl/fl^ OIR mice), P17 (**b**, **e**, **h**) (*n* = 9 *Aggf1*^fl/fl^ and 12 *Cdh5-Cre Aggf1*^fl/fl^ OIR mice) and P21 (**c**, **f**, **i**) (*n* = 5 *Aggf1*^fl/fl^ and 4 *Cdh5-Cre Aggf1*^fl/fl^ OIR mice). In the inserts, the red line represents the edge of the retina, the blue area represents the avascular

area, and the red area represents NVTs. **j** TER119-positive RBC leakage in *Aggf1*^fl/fl^ and *Cdh5-Cre Aggf1*^fl/fl^ OIR mice are shown (*n* = 5 mice per group). **k** F4/80-positive macrophage infiltration in *Aggf1*^fl/fl^ and *Cdh5-Cre Aggf1*^fl/fl^ OIR mice are shown (*n* = 5 mice per group). Error bars represent mean ± SEM. 2-tailed unpaired Student's *t* test (**g**, **h**, **i**). Scale bars: 1000 µm (**a**–**f**) and 100 µm (**j**, **k**). Source data are provided as a Source Data file.
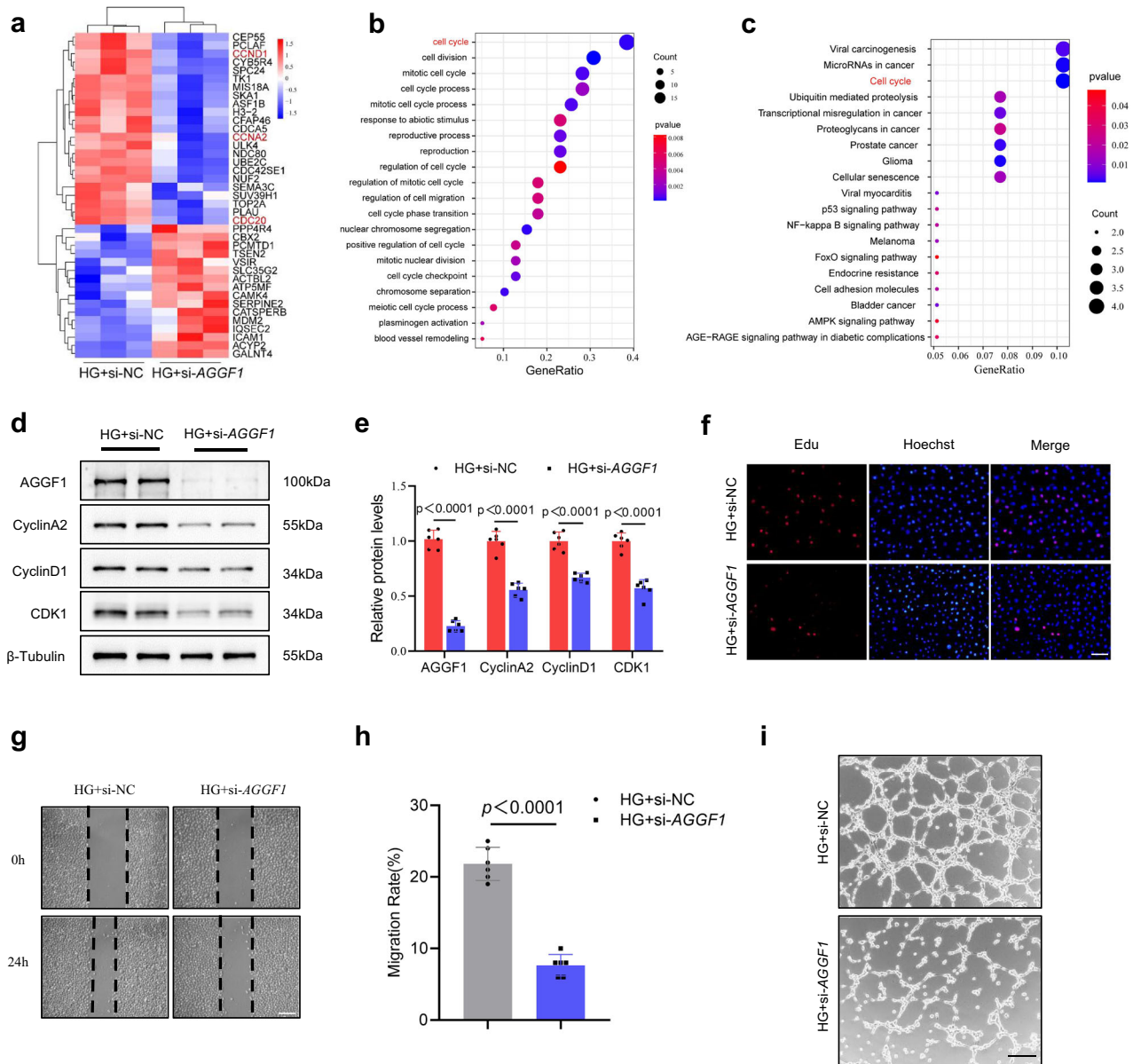
Fig. 4 | AGGF1 promoted angiogenesis by upregulating proliferation-related indicators. a Heat maps from proteomic array analysis with ranked enriched genes between control and *AGGF1*-silenced HRMECs treated with HG (fold-change >1.2 or <0.83, *p* < 0.05). High and low expression are denoted by red and navy, respectively (*n* = 3 independent cultures). **b**, **c** GO terms and KEGG pathway analysis of the differentially expressed genes between control and *AGGF1*-silenced HRMECs treated with normal glucose and HG. Statistical analysis was performed using Fisher exact test. **d**, **e** Western blot analysis and quantification of AGGF1, CyclinA2, CyclinD1 and CDK1 protein levels in control and *AGGF1*-silenced HRMECs treated with HG (*n* = 6 independent cultures). **f** Cell proliferation was performed by EdU staining of control and *AGGF1*-silenced HRMECs treated with HG (*n* = 3 independent cultures). **g**, **h** Representative images and quantification of control and *AGGF1*-silenced HRMECs treated with HG in wound healing assay at 0 and 24 h (*n* = 3 independent cultures). **i** Representative images of angiogenesis in control and *AGGF1*-silenced HRMECs treated with HG, measured using in vitro tube formation assays (*n* = 3 independent cultures). Error bars represent mean ± SEM. 2-tailed unpaired Student's *t* test (**a**, **e**, **h**). Scale bars: 100 μm (**f**, **i**), 1000 μm (**g**). HG high glucose (33.3 mmol/L). Source data are provided as a Source Data file.

to FN14 diminished when *AGGF1* was silenced (Fig. 5m and Supplementary Fig. 17a). Taken together, these results provide evidence that AGGF1 promotes the binding of TNFSF12 to Fn14 to increase angiogenesis.

Anti-AGGF1 therapy inhibited retinal pathological neovascularization
Our initial results demonstrated that endothelial AGGF1 depletion reduced pathological angiogenesis in ischaemic retina. To further clarify whether local AGGF1 depletion produces therapeutic effects in OIR mice, we intravitreally injected 2.5 μL of anti-AGGF1 antibody or anti-IgG antibody into C57BL/6J OIR mice at P13 and

isolated the retinas at P17 (Fig. 6a). The NVT and avascular areas decreased in OIR mice intravitreally injected with the anti-AGGF1 antibody compared to those in mice intravitreally injected with the anti-IgG antibody (Fig. 6b–d). TNFSF12 binds to AGGF1 to form complexes mediating AGGF1 downstream signal transduction, which are related to angiogenesis. To elucidate whether local TNFSF12 depletion has therapeutic effects in OIR mice, we neutralised TNFSF12 through intravitreal injection. The avascular area of OIR mice intravitreally injected with anti-TNFSF12 antibody was decreased compared with that of mice injected with anti-IgG antibody (Fig. 6b–d and Supplementary Fig. 18a–c). Simultaneous injection of AGGF1 and TNFSF12 antibodies was more effective than
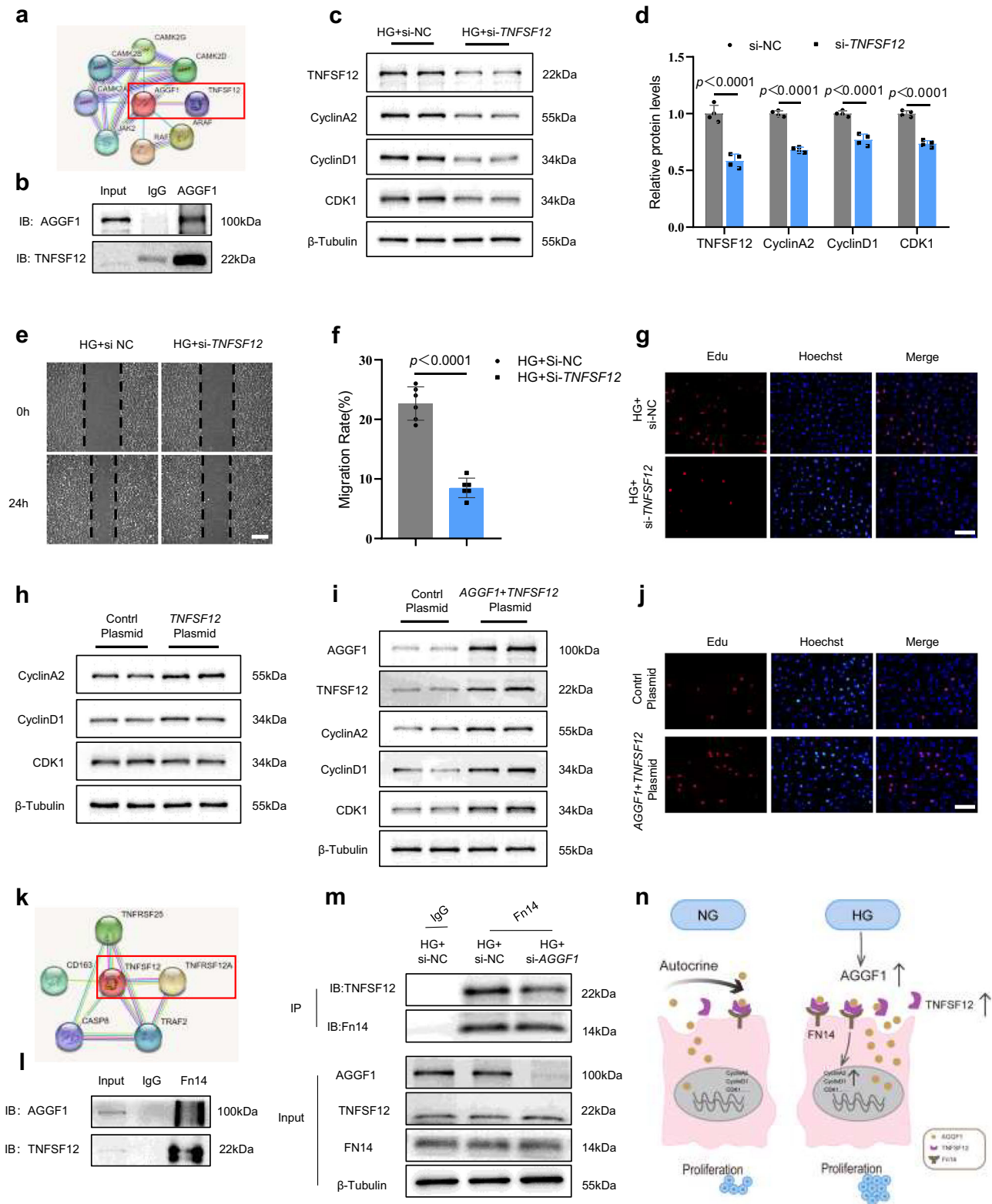
either antibody alone in reducing NVT and avascular areas (Fig. 6b–d and Supplementary Fig. 18a–c), as expected. Overall, these findings provide evidence that AGGF1 is critical for endothelial signal transduction in retinal pathological angiogenesis. They also imply that anti-AGGF1 therapy can serve as a promising treatment target for improving retinal pathological angiogenesis in

OIR. Moreover, it was found that AGGF1 + VEGF blockade was more effective than either treatment alone in ameliorating pathological angiogenesis (Fig. 6b–d and Supplementary Fig. 18a–c). These findings provide evidence that simultaneous targeting of AGGF1 and VEGF produces a synergistic anti-angiogenic effect in the ischaemic retinopathy.

Fig. 5 | AGGF1 promoted the binding of TNFSF12 to Fn14 to increase angiogenesis. a AGGF1 protein interaction network analysed by STRING (string-db.org). **b** Immunoprecipitated (IP) AGGF1 was immunoblotted (IB) with AGGF1 or TNFSF12 antibody in HRMECs. **c, d** Western blot analysis and quantification of TNFSF12, CyclinA2, CyclinD1, and CDK1 protein levels in control and *TNFSF12*-silenced HRMECs treated with HG ($n = 4$ independent cultures). **e, f** Representative images and quantification of control and *TNFSF12*-silenced HRMECs treated with HG (Scratching wound healing assay) ($n = 6$ independent cultures). **g** Representative images of control and *TNFSF12*-silenced HRMECs treated with HG (EdU staining) ($n = 3$ independent cultures). **h** Western blot analysis of CyclinA2, CyclinD1, CDK1, and TNFSF12 protein levels in blank control and *TNFSF12*-plasmid HRMECs ($n = 6$ independent cultures). **i** Western blot analysis of CyclinA2, CyclinD1, CDK1, AGGF1, and TNFSF12 protein levels in blank control and *AGGF1 + TNFSF12*-plasmid HRMECs ($n = 4$ independent cultures). **j** Representative images of blank control and *AGGF1 + TNFSF12*-plasmid HRMECs (EdU staining) ($n = 3$ independent cultures). **k** TNFSF12 protein interaction network analysed by STRING (string-db.org). **l** Immunoprecipitated (IP) FN14 immunoblotted (IB) with AGGF1 or TNFSF12 antibody in HRMECs. **m** Immunoprecipitated (IP) FN14 immunoblotted (IB) with TNFSF12 or FN14 antibody in HRMECs treated with HG. **n** Schematic illustration of AGGF1 promoting the binding of TNFSF12 to Fn14 to increase angiogenesis. Error bars represent mean ± SEM. one-way ANOVA with Tukey's multiple comparisons test (**d, f**). Scale bars: 1000 μm (**e**) and 100 μm (**g, j**). HG, high glucose (33.3 mmol/L). Source data are provided as a Source Data file.

SGLT2i reduced pathological neovascularisation by decreasing AGGF1

Our study showed that elimination of endogenous AGGF1 in the retina had a therapeutic effect following OIR, demonstrating that endothelial AGGF1 deficiency promotes healthy retinal angiogenesis and abnormal vessel regression in the ischaemic retina. Studies have shown that sodium-glucose cotransporter 2 inhibitors (SGLT2i) attenuates proliferation and angiogenesis in hepatocellular carcinoma cells[41]. To explore the beneficial effects of SGLT2i on the retina, we observed changes after administration of SGLT2i in vivo and in vitro. The results showed that retinal thickness was significantly greater in db/db mice than age-matched db/db+SGLT2i mice (Fig. 7a–c). Retinal trypsin digestion assays showed that the number of acellular capillaries was markedly decreased in db/db+SGLT2i mice (Fig. 7d and Supplementary Fig. 19a). These data demonstrated that SGLT2i had a protective effect against DR. We then determined whether SGLT2i had a protective effect through the AGGF1 signalling pathway. The expression of AGGF1 was significantly lower in db/db+SGLT2i mice than in db/db mice (Fig. 7e–g and Supplementary Fig. 20a and Supplementary Data 3). Western blot analysis revealed a significant decrease in the expression of cell cycle proteins after SGLT2i (Fig. 7h–k). In addition, cell proliferation and migration abilities were significantly recovered in HRMECs exposed to the SGLT2i compared to those exposed to HG (Fig. 7l–n). Collectively, these data demonstrate that SGLT2i achieved a therapeutic effect by early inhibition of the AGGF1 signalling pathway and imply that AGGF1 depletion could be a promising treatment strategy for preventing the exacerbation of ischaemic retinal vasculopathy, such as in DR.

Discussion

Although anti-VEGF therapy is the primary therapeutic approach for retinal vasculopathy, its clinical efficacy remains suboptimal. Impaired retinal vascularisation in ischaemic retinopathy leads to excessive retinal vascularization, which the metabolic equilibrium. Therefore, there is an urgent need to identify novel antiangiogenic targets. Our findings revealed that in PDR, AGGF1 was elevated in the vitreous fluid, whereas endothelial AGGF1 deficiency ameliorated pathological angiogenesis in an OIR model. Mechanistically, AGGF1 expression in ECs was regulated by retinal hypoxia caused by pathological changes. Our findings also suggest a mechanism of action by which AGGF1 promotes angiogenesis by activating the cell cycle via the TNFSF12/FN14 signalling pathway (Fig. 8).

Notably, in the proliferation stage of OIR mice, AGGF1 expression was enhanced immediately, which was consistent with VEGF expression. Notably, these results are in line with the role of VEGF in mediating retinal neovascularisation and vascular leakage under hypoxic conditions[42]. In this study, we found that *AGGF1* loss in retinal ECs notably decreased retinal vaso-occlusion, neovascularisation, and vascular leakage during angiogenesis. Therefore, we hypothesised that AGGF1 is a potent factor that promotes pathological angiogenesis in retinopathy. AGGF1 is highly expressed in tumours and regulates tumour angiogenesis[25], and increases the binding of TNFSF12 to FN14 to promote angiogenesis[21]. Previous studies further support our hypothesis that AGGF1 is a critical angiogenic factor in excessive angiogenesis.
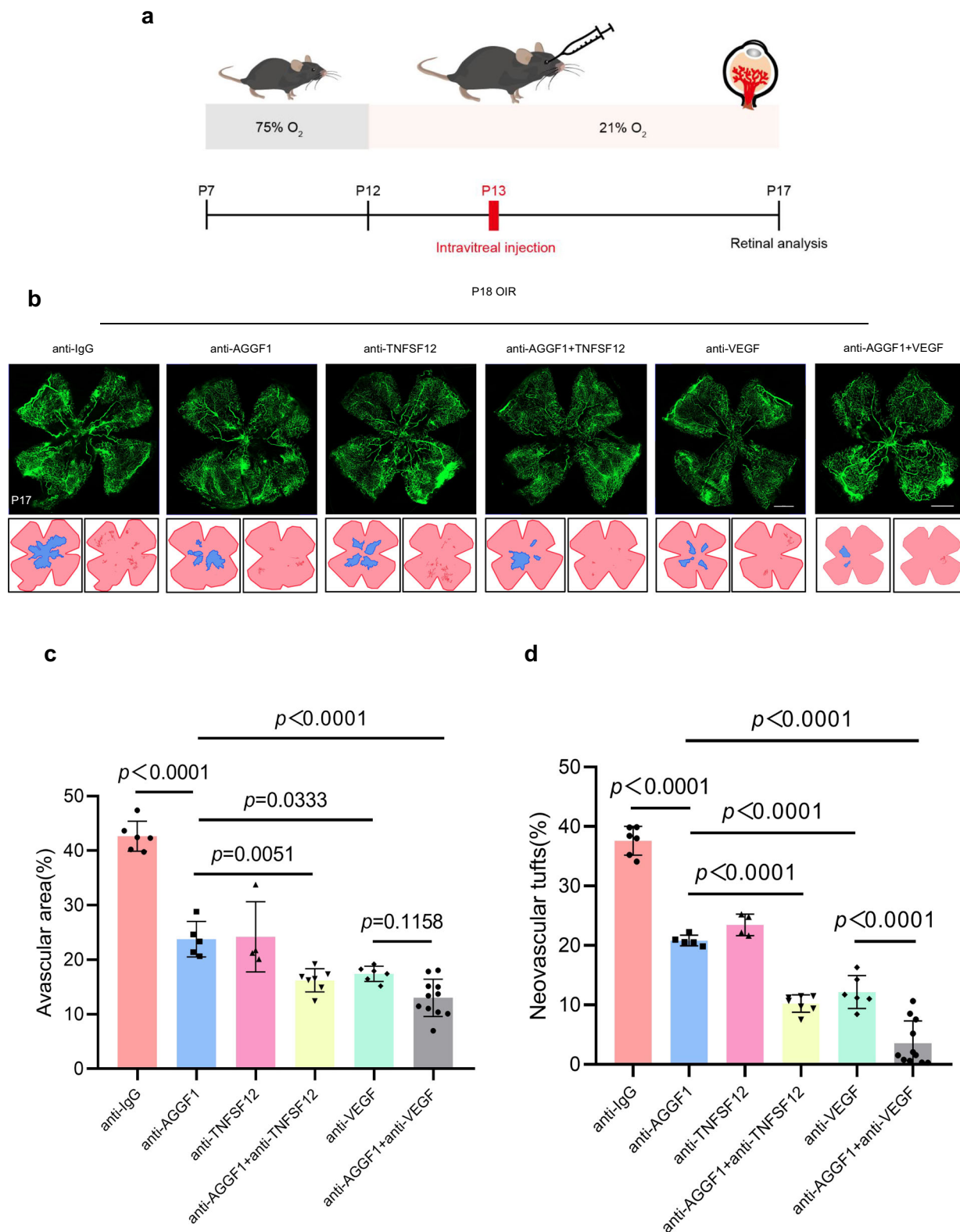
Notably, intravitreal injection of an anti-AGGF1 antibody effectively prevented excessive pathological angiogenesis in OIR mice in this study. It is known that hypoxia-induced VEGF expression plays a key role in inducing retinal angiogenesis[43,44]. Intravitreal therapies targeting VEGF have shown remarkable clinical efficacy[16,45,46]. However, anti-VEGF treatment is ineffective in patients with retinal vascular diseases[20,47]. AGGF1 is not the same as VEGF; it is mainly engaged in EC proliferation and migration and has a more potent pro-angiogenic effect[25]. In this study, we found that the simultaneous targeting of AGGF1 and VEGF produces synergistic effects in the treatment of retinal vascular diseases.

Proliferative retinopathy is characterised by ischaemia-induced neovascularisation regulated by the HIF pathways[34]. Previous studies have suggested that hypoxia stimulates HIF expression. HIFs play a central role in the regulation of a range of proangiogenic genes, such as those involved in vascular permeability, angiogenesis, and oxygen homeostasis[33]. Interestingly, we found that HIF-1α expression was elevated in HRMECs exposed to HG. And it also increased AGGF1 expression in HG-exposed HRMECs. We further assessed the central role of HIF-1α, which promoted AGGF1 expression by directly binding to the AGGF1 promoter. This could explain why AGGF1 expression increased not only in HG but also under hypoxia.

The TNFSF12/FN14 complex is known to promote angiogenesis. In this study, we revealed that the activation of the AGGF1/TNFSF12/FN14 signalling pathway promotes retinal pathological angiogenesis. Previous studies have indicated that TNFSF12 enhances cell proliferation, migration and angiogenesis[40,48–50]. Similarly, TNFSF12 protein expression was increased in the retinas of OIR mice in this study. We also found that TNFSF12 enhanced the pro-angiogenic effects of AGGF1 in vitro and in vivo, further elucidating the importance of TNFSF12 in mediating retinal pathological neovascularisation. Moreover, our study showed that intravitreal injection of anti-TNFSF12 antibody in OIR mice reduced vaso-obliteration and neovascularisation similar to the previously reported phenotype of *Cdh5-Cre Aggf1^{fl/fl}* OIR mice. Thus, our results uncovered the effects of AGGF1/TNFSF12/FN14 on the regulation of retinal neovascular diseases.

We also found that AGGF1 was required for retinal angiogenesis by activating the cell cycle. Cell cycle proteins play important roles in various developmental and pathological processes. Our findings illustrate that the co-overexpression of AGGF1 and TNFSF12 in ECs distinctively increased cell cycle protein expression, accompanied by excessive angiogenesis. This abnormal reaction in ECs can be reversed by knockout of AGGF1 or TNFSF12 via inactivation of the cell cycle. Collectively, our data suggest that endothelial AGGF1 promotes pathological retinal angiogenesis by activating the cell cycle.

SGLT2i is a commonly used hypoglycaemic agent that is widely used in diabetic nephropathy and diabetic cardiomyopathy. However, the question remains whether it is beneficial for diabetic retinopathy.

Fig. 6 | Anti-AGGF1 treatment inhibits retinal angiogenesis. a Schematic illustration of the OIR mice treated with intravitreal injections. At P13, mouse pups were intravitreally injected with 2.5 μL anti-IgG, anti-AGGF1, anti-TNFSF12, anti-AGGF1 + TNFSF12, anti-VEGF, or anti-AGGF1 + VEGF antibodies. Retinas were analysed at P17. **b–d** FITC-dextran staining of whole-mount retinas from OIR mice injected with anti-IgG ($n = 6$ mice), or anti-AGGF1 antibody ($n = 5$ mice), or anti-TNFSF12 antibody ($n = 4$ mice), or anti-AGGF1 + TNFSF12 antibody ($n = 7$ mice), or anti-VEGF antibody ($n = 6$ mice), or anti-AGGF1 + VEGF antibody ($n = 11$ mice). In the inserts, the red line represents the edge of the retina, the blue area represents the avascular area, and the red area represents NVTs. **c, d** Quantification of the avascular and NVT areas at P18 in OIR mice, related to B. Error bars represent mean ± SEM. one-way ANOVA with Tukey's multiple comparisons test (**c, d**). Scale bars: 1000 μm (**b**). Source data are provided as a Source Data file.
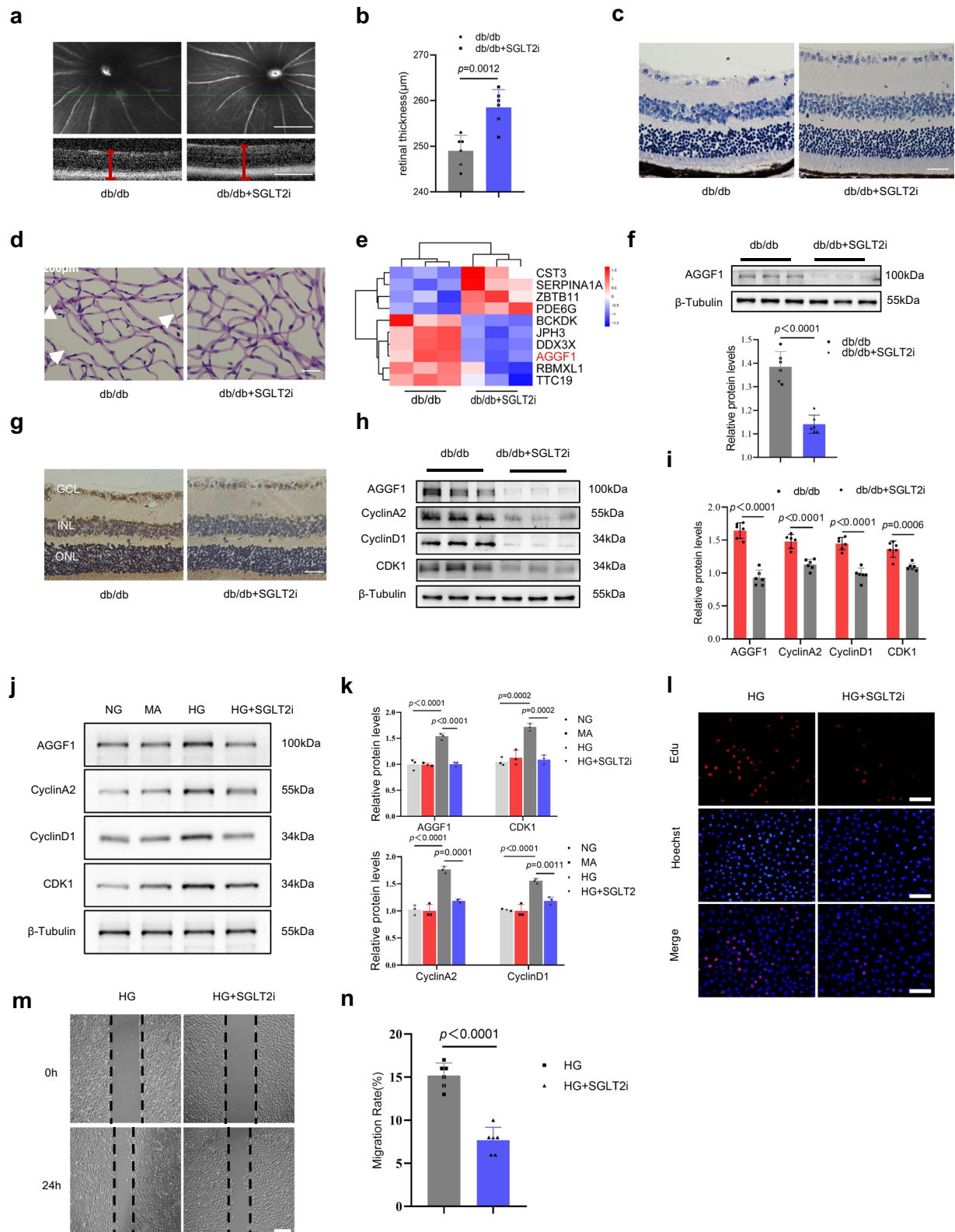
Recently, many studies have shown that SGLT2i is effective in delaying the progression of diabetic retinopathy[51–56]. Dapagliflozin, a potent and selective hSGLT2 inhibitor, may prevent preclinical DR[57]. Our study discovered a pathway affected by SGLT2i. Our study found that AGGF1 was already higher than the controls in the aqueous humour of diabetic patients, suggesting that once diabetes progresses, AGGF1 increases. Meanwhile, it was observed that SGLT2i could reduce AGGF1

and cell cycle proteins at an early stage. Therefore, SGLT2i is expected to reduce the expression level of AGGF1 at an early stage of diabetes and thus slow the progression of diabetic retinopathy.

Notably, we found that AGGF1 was expressed in both macrovascular and microvascular vessels in P17 OIR mouse retinas, whereas we usually think that angiogenesis typically occurs in the microvasculature. A limitation of our study is that we only focused on the

Fig. 7 | SGLT2i reduced pathological neovascularisation by decreasing AGGF1.
a, **b** Fundus and OCT cross-sectional structural images and quantification of the retinal thickness measured by OCT in db/db mice compared to those in age-matched db/db+SGLT2i (Dapagliflozin, 1.5 mg/kg/d) mice (*n* = 6 mice per group). **c** Paraffin HE staining for retinal thickness in db/db mice and db/db+SGLT2i mice (*n* = 4 mice per group). **d** PAS staining of retinal trypsin digestion visualizing retinal vasculature and acellular capillaries (white arrowheads) in db/db mice and db/db +SGLT2i mice (*n* = 5 mice per group). **e** Heat maps from proteomic array analysis with ranked enriched genes in 3 db/db mice and 3 db/db+SGLT2i mice retinas (fold-change >1.2 or <0.83, *p* < 0.05). High and low expression are denoted by red and navy, respectively. **f** Western blot analysis and quantification of AGGF1 protein levels in the retinas of db/db and db/db+SGLT2i mice (*n* = 6 mice per group). **g** Immunohistochemical detection of AGGF1 expression in db/db and db/db +SGLT2i mice (*n* = 3 mice per group). **h**, **i** Western blot analysis and quantification

of AGGF1, CyclinA2, CyclinD1 and CDK1 protein levels in the retinas of db/db and db/db+SGLT2i mice (*n* = 6 mice per group). **j**, **k** Western blot analysis and quantification of AGGF1, CyclinA2, CyclinD1 and CDK1 protein levels in NG, MA, HG and HG+SGLT2i HRMECs (*n* = 3 independent cultures). **l** Representative images of HRMECs treated with HG and HG+SGLT2i was performed by EdU staining to reflect cell proliferation (*n* = 3 mice per group). **m**, **n** Representative images and quantification of HRMECs treated with HG and HG+SGLT2i in wound healing assay at 0 and 24 h (*n* = 6 independent cultures). Error bars represent mean ± SEM. 2-tailed unpaired Student's *t* tests (**b**, **f**, **i**, **k**). Scale bars: 50 μm (**c**, **d** and **g**); 100 μm (**l**), 1000 μm (**m**). NG normal glucose (5.5 mmol/L glucose), MA mannitol (5.5mmol/L glucose+ 27.8 mmol/L mannitol), HG high glucose (33.3 mmol/L glucose), SGLT2i SGLT2 inhibitors (Dapagliflozin), GCL ganglion cell layer, INL inner nuclear layer, ONL outer nuclear layer. Source data are provided as a Source Data file.
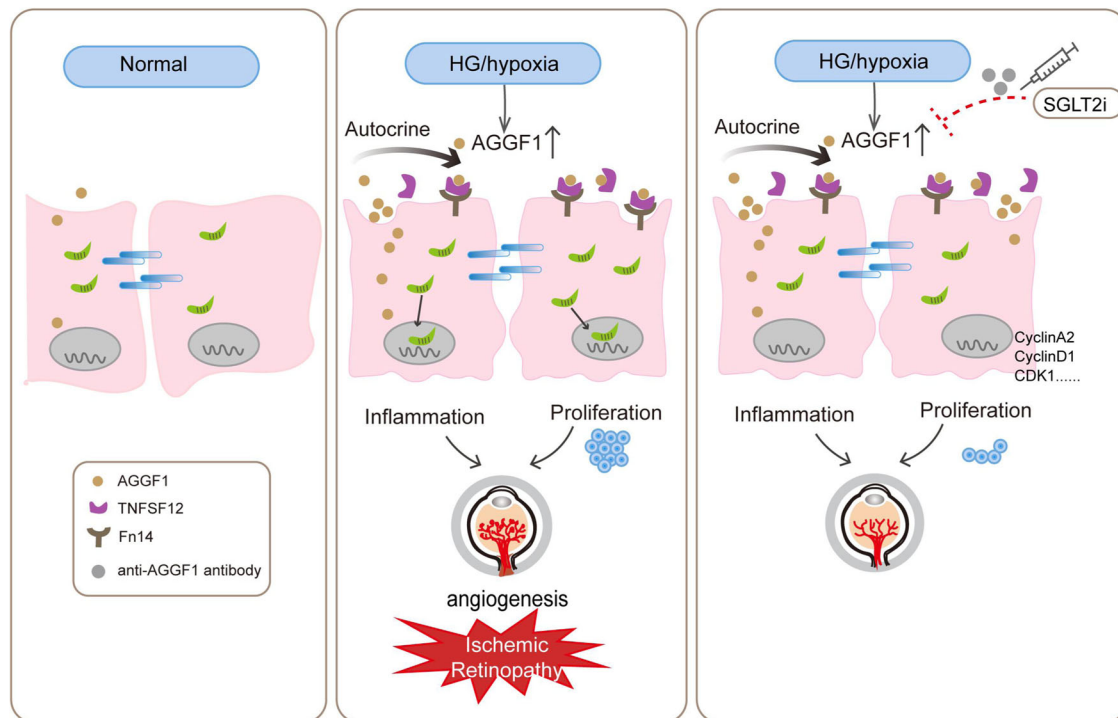
Fig. 8 | Schematic illustration of the mechanism by which endothelium-derived AGGF1 attenuates ischaemic retinopathy. Endothelial AGGF1 deficiency ameliorates pathological angiogenesis in an OIR model. Mechanistically, AGGF1 expression in HRMECs is regulated by retinal hypoxia caused by pathological changes. Our

study also suggests an action model through which AGGF1 promotes angiogenesis by activating the cell cycle via the AGGF1/TNFSF12/FN14 signalling pathway. Thus, we speculate that targeting the AGGF1/TNFSF12/FN14 signalling pathway could provide a therapy for the treatment of ischaemic retinopathy.

role of AGGF1 in microvessels to promote angiogenesis in retinas; thus, the role of AGGF1 in macrovessels requires further exploration. In our study, we observed that the number of F4/80-postive macrophages was significantly reduced in the *Cdh5-Cre Aggf1fl/fl* OIR mice retinas compared to that in *Aggf1fl/fl* OIR mice at P17, suggesting that AGGF1 may be involved in the regulation of retinal inflammation. Therefore, the role of AGGF1 played in retinal inflammation warrants further investigation.

We demonstrated in vivo, for the first time, the physiological functions of AGGF1 in vascular development using endothelial-specific *Aggf1* knockout mice and further revealed the angiogenic effect of AGGF1 in pathological processes. We demonstrated that the AGGF1/TNFSF12/FN14 signalling pathway plays an essential role in pathological angiogenesis during ischaemic retinopathy. Thus, we speculate that targeting the AGGF1/TNFSF12/FN14 signalling pathways could provide a therapeutic strategy for treating ischaemic retinopathy.

Methods
Patient samples
All the patients provided written informed consent for the procedure, and the participation of the study. Vitreous fluid samples were obtained from patients with PDR who underwent vitrectomy or from non-diabetic patients without vascular disease. The vitreous was placed on a 4 °C ice box after vitrectomy and then immediately transferred to a −80 °C refrigerator for storage. Aqueous humour samples were obtained from patients with PDR who received intravitreal anti-VEGF drug injections or from nondiabetic patients who underwent cataract surgery. The aqueous humour was placed on a 4 °C ice box after collection and stored at −80 °C.

Animals
Endothelium-specific *Aggf1* homozygous-deficient (*Cdh5-Cre Aggf1fl/fl*) mice were generated by crossbreeding *Aggf1fl/fl* and Cdh5-Cre mice. For comparison, *Aggf1fl/fl* and *Cdh5-Cre Aggf1fl/fl* littermates were used as

controls. Male leptin receptor-mutant (db/db) mice and age-matched db/m mice were used in the same experiments. Db/db mice and db/m mice were obtained from Gem Pharmatech (Jiangsu, China), and *Aggf1*^{fl/fl} and *Cdh5-Cre Aggf1*^{fl/fl} mice were obtained from Cyagen (Jiangsu, China). All mice were housed in the standard, purpose-built, pathogen–free, institutional animal care-facility of the Tianjin Medical University (Tianjin, China). Mice were kept in a 12 h light/dark cycle and 10% humidity at $20 \pm 4\,°C$. They were given free access to chow and water. All animal experiments strictly complied with the National Institutes of Health Guide for *the Care and Use of Laboratory Animals*. All animal experimental protocols were approved by the Laboratory Animal Ethics Committee of Tianjin Medical University Chu Hsien-I Memorial Hospital. We selected 14-week-old db/m and db/db mice for our experiments. Mice in the db/db+SGLT2i group were orally administered dapagliflozin (1.5 mg/kg/d) for 12 weeks. The concentration of dapagliflozin was converted based on the instructions provided for humans (maximum dosage, 10 mg/day) according to body surface area.

Assessment of protein levels by ELISA
Concentrations of AGGF1 and VEGFA protein in human aqueous humours were measured using a human AGGF1 ELISA kit (ELISA LAB, JYM2912Hu), and a human VEGFA ELISA kit (ELISA LAB, JYM0103Hu) according to the manufacturer's instructions.

Oxygen-induced retinopathy mouse model
To induce vaso-obliteration, P7 pups and breeding mothers were housed in an oxygen chamber under hyperoxia (75% oxygen) until P12. At P12, the pups were housed under normoxic conditions (21% oxygen) until P17. Age-matched mice placed under normoxic conditions were used as controls[31]. Aggf1 knockout OIR mice were compared to littermate controls. All the retinas were harvested at P12, P17 and P21.

Fluorescein isothiocyanate (FITC)-conjugated dextran staining of whole-mount retinas
OIR mice were anesthetized, the heart was exposed, FITC-dextran (50 mg/ml, Sigma FD2000S) was injected into the left ventricle, and the eye was removed and placed in 4% paraformaldehyde (PFA) for fixation for at least 40 minutes. The retinal pavement was peeled and photographed using an organ confocal microscope. The FITC-dextran method was used to label the retinal vasculature and to assess the retinal avascular area and neovascular tufts.

Cell culture and treatments
Human retinal microvascular endothelial cells (HRMECs) were acquired from BNCC (BeNa Culture Collection) and cultured in Endothelial Cell Medium (ECM, ScienCell, USA) containing a low concentration of foetal bovine serum (5%) at $37\,°C$ in 5% CO_2. HRMECs were inoculated in 6-well plates and treated with high concentrations of D-glucose until the cell density reached approximately 70%. The same concentration of D-mannitol was used as the control for osmolality. According to the CCK-8 assay, we selected 10 μmol/L for 48 h as the testing concentration of Dapagliflozin in our in vitro study (Supplementary Fig. 21a).

Si-RNA transfection
Transfection of *AGGF1*, *TNFSF12* or *HIF1A* siRNA, and *AGGF1* or *TNFSF12* plasmid (RiboBio, Guangzhou, China) was performed using the INVI DNA RNA Transfection reagent™ (Invitrogen, USA) according to, the manufacturer's protocols. All siRNA sequences are listed in Supplementary Table 4.

Optical coherence tomography
After the mice were anaesthetised, the pupils were dilated and antibiotic ointment was applied to prevent drying of the eyes. The mice were placed on the small animal retinal fibre imager stand, and one operator operated the instrument and positioned the mice correctly. The other operator operated the computer and adjusted the sharpness after finding a suitable field of view, and took pictures immediately[58]. Retinal thickness was assessed using OCT (Heidelberg, Germany) and statistical analysis was performed using the GraphPad Prism software (version 8.0).

Haematoxylin and eosin (HE) staining
Paraffin sections (4 μm) were dewaxed in xylene, rehydrated in graded alcohol, sequentially stained with haematoxylin and eosin[59], and viewed under a light microscope (Olympus BX53, Japan).

Retinal trypsin digestion
Retinal trypsin digestion was performed to analyse the retinal vasculature. The eyeballs were fixed in 4% PFA for two days. Retinas were dissected and washed in ddH_2O water overnight. The next day, the retinas were incubated with 3% trypsin (Scientific Phygene, PH9033) for 3 h at $37\,°C$ and shaken gently to isolate the vascular network from adherent retinal tissue. The cells were then stained with periodic acid Schiff (PAS), and histopathological changes in the retinal vasculature were observed under a light microscope (Olympus BX53, Japan). The number of acellular capillaries was counted in five random fields.

Proteomic array analysis
We performed a proteomic analysis of the retinas of db/m, db/db, and db/db+SGLT2i mice at 20 weeks of age, and generated heatmaps and volcano plots. We performed proteomic analysis of the human retinal microvascular endothelium enriched for HG+si-NC and HG+si-*AGGF1*, and generated heatmaps and volcano plot.

In the bioinformatics analysis of the article, all differential proteins are included. We have provided supplementary excel containing all proteins identified in each sample and their fold-change (FC) and *P* values. The statistical analysis was performed by t-tests and proteins with FC greater than 1.2 times (upregulation greater than 1.2 times or downregulation less than 0.83 times) and p values less than 0.05 ($p < 0.05$) were determined as a significant difference.

Retinas and cells were lysed and protein extraction with SDT buffer (4% SDS, 100 mM Tris-HCl, 1 mM DTT, pH 7.6). The amount of protein was quantified with the BCA Protein Assay Kit (Bio-Rad, USA). Protein trypsin digestion was performed according to filter-aided sample preparation (FASP) procedure described by Matthias Mann[60]. The digest peptides were desalted on C18 Cartridges (Empore™ SPE Cartridges C18 (standard density), bed I.D. 7 mm, volume 3 ml, Sigma), concentrated by vacuum centrifugation and reconstituted in 40 μl of 0.1% formic acid. The extracted proteins were mixed with 5X loading buffer and separated on SDS-PAGE gel. Protein bands were visualized by Coomassie Blue R-250 staining. Then 100 μg peptide mixture of each sample was labelled using TMT reagent according to the manufacturer's instructions (Thermo Scientific). Labelled peptides were fractionated by High pH Reversed-Phase Peptide Fractionation Kit (Thermo Scientific). LC-MS/MS analysis was performed on a Q Exactive mass spectrometer (Thermo Scientific) that was coupled to Easy nLC (Proxeon Biosystems, now Thermo Fisher Scientific). The MS raw data for each sample were searched using the MASCOT engine (Matrix Science, London, UK; version 2.2) embedded into Proteome Discoverer 1.4 software for identification and quantitation analysis.

Bioinformatic analysis
Firstly, normalize the quantitative information of the protein set to the (−1,1) interval. Then Using the Complexheatmap R package (R Version 3.4) to classify the expression levels of samples and proteins in two dimensions (distance algorithm: Euclidean, connection method: Average linkage) Gene ontology (GO) terms were mapped and

sequences were annotated using the software program Blast2GO, and Use KAAS (KEGG Automatic Annotation Server) to annotate the target protein set for KEGG pathway. Finally, these results were drawn in R language.

Immunostaining of whole-mount retinas

At P17, whole eyeballs were harvested and placed in 4% PFA for fixation. After being washed in filtered PBS, the retinas were isolated and placed in 4% PFA overnight at 4 °C. Retinas were washed twice in PBS and placed in permeable buffer (PBS pH 6.8, 1% BSA, 0.5% TritonX-100) overnight at 4 °C[61]. Then, isolectin B4 (1:200, Invitrogen, I21411) staining with different primary antibodies against AGGF1 (1:200, Novus, NB100-455), GFAP (1:200, Proteintech, 60190-1-Ig), Iba-1 (1:200, Abcam, ab283319), TER119 (1:100, Invitrogen, 14-5921-81), and F4/80 (1:200, Proteintech, 28463-1-AP) was performed overnight at 4 °C. The following day, the retinas were incubated with the appropriate fluorescently labelled secondary antibodies (1:200, SIMUBIOTECH, S2003) for 2 h at room temperature. Finally, retinas were washed and spread on microscope slides. Images were captured using a laser-scanning confocal microscope (Zeiss LSM 800, Germany).

Quantification of avascular and NVTs areas in OIR retinas

All the FITC-dextran images were imported into Photoshop CS6 (Adobe Systems) for analysis. The entire retinal area was marked using the magnetic lasso tool to mark the non-perfused retinal area using the Quick Selection tool. The pathological neovascularisation area was marked using the magic wand tool, and all values were expressed as pixel values. Finally, the perfusion-free area/retinal area and pathological neovascularisation/retinal area ratios were analysed.

Intravitreal injections

During the experiment, the pups were deeply anesthetised and placed on a thermos-controlled heating pad to maintain their body temperature. A Hamilton syringe was inserted into the vitreous cavity at a 45° angle at the posterior edge of the cornea and held in place for 30 s prior to injection[62]. *Aggf1*$^{fl/fl}$ or *Cdh5-Cre Aggf1*$^{fl/fl}$ mice were injected with 2.5 μL of anti-IgG (1:50, Cell Signalling Technology, 2729 s) or anti-TNFSF12 (1:50, Proteintech, 12537-1-AP), respectively. Additionally, 2.5 μL of anti-IgG, anti-AGGF1 (1:50, Proteintech, 11889-1-AP), anti-TNFSF12 (1:50, Proteintech, 12537-1-AP), or anti-VEGF (1:50, Proteintech, 19003-1-AP) was injected into C57BL/6 mice, respectively. An antibiotic ointment was applied to the surface of the eyes to prevent corneal dryness and intraocular infections after the intravitreal injections. We administered the injections at P13 and harvested and analysed the retinas at P17.

Western blotting

Retinas and cells were collected on ice by adding RIPA lysis buffer (Solarbio, China) containing protease inhibitors to extract total proteins. The proteins were then separated by SDS/PAGE and transferred onto nitrocellulose membranes. After blocking with 5% skim milk for 1 h, membranes were incubated with anti-AGGF1 (1:1000, Proteintech, 11889-1-AP), anti-VEGF (1:1000, Proteintech, 19003-1-AP), anti-TNFSF12 (1:500, Proteintech, 12537-1-AP), anti-FN14 (1:1000, ABclonal, A5955), anti-CyclinA2 (1:3000, Proteintech, 18202-1-AP), anti-CyclinD1 (1:5000, Proteintech, 60186-1-Ig), anti-CDK1 (1:1000, Proteintech, 19532-1AP), anti- HIF-1α (1:1000, Proteintech, 20960-1-AP), and anti-β-Tubulin (1:5000, Bioworld, AP0064) antibodies, followed by HRP-conjugated secondary anti-rabbit/mouse antibodies (1:5000, Sungene Biotech). The band intensity was determined using an enhanced ECL kit (WBKLS0500; Millipore) and quantified using ImageJ software. Data were normalised to β-tubulin expression.

Tube formation assay

The Matrigel matrix glue was dissolved overnight. Precooled Matrigel matrix gel was added to 24-well plates and solidified for 30 minutes at 37 °C. HRMECs were plated in 24-well plates and incubated at 37 °C in a 5% CO_2 incubator. The capillary tube was imaged using a bright-field microscope (Olympus IX83, Japan).

Scratch wound healing assay

HRMECs were inoculated into 6-well plates. After intervention, cell cultures were scratched with a 100 μL transfer liquid gun and then washed three times in PBS to remove the delimit cells and continue the culture. The cell scratches were photographed and measured using a light microscope (Olympus IX83, Japan) at 0 h and 24 h.

EdU assay

EdU staining was performed using the Click-It EdU kit (Bioscience, Shanghai, China). In short, HRMECs were plated in 24-well plates and incubated with EdU for 2 h at 37 °C. The cells were then fixed in 4% PFA for 30 min (residual paraformaldehyde was neutralised in a glycine solution) and washed twice with 3% BSA. Next, the cells were permeabilised in 0.5% Triton X-100 for 20 min and incubated in Click-iT reaction solution for 30 min at room temperature, followed by Hoechst 33342-stained nuclei for 20 min. Images were captured by using an inverted fluorescence microscope (Olympus IX83, Tokyo, Japan).

Co-IP

An immunoprecipitation kit (Thermo Fisher Scientific, CA, USA) was used to investigate the interactions between AGGF1 and TNFSF12, AGGF1 and FN14, TNFSF12 and FN14. HRMEC lysates were prepared in RIPA buffer (SolarBio, China). Dynabeads® Protein A (bimake.cn, B23202) was incubated with anti-AGGF1 antibody [immunoglobulin G (IgG) as a control] for 3 h and incubated with the cell lysate supernatants overnight at 4 °C. The precipitates were washed and eluted by boiling in 1× SDS loading buffer, after which they were used for western blotting.

Immunohistochemistry

After dewaxing, gradient rehydration, and high-temperature antigen repair, the retinal slices were blocked with 3% hydrogen peroxide solution for 15 min and then with 10% goat serum (Sigma, USA) for 30 min. Next, the retinal slices were incubated with the corresponding primary antibody against AGGF1 (1:200, Novus, NB100-455) overnight at 4 °C. The next day, retinal slices were incubated with an HRP-conjugated secondary antibody (Zsbio, China). Retinal sections were stained using a diaminobenzidine (DAB) kit (Zsbio, China), and nuclei were stained with haematoxylin. The images were captured using a bright-field microscope (Olympus BX53, Japan).

Immunofluorescence staining

The HRMECs were cultured and processed in 12-well plates. The cells were incubated with 4% PFA for 30 min at room temperature, permeabilised with 0.1% Triton X-100 (Solarbio, China) for 30 min, and blocked with 10% goat serum (Sigma, USA) for 1 h. HRMECs were then incubated with anti-CD31 primary antibody (1:200, Proteintech, 11265-1-AP) at 4 °C overnight. The next day, the HRMECs were incubated with FITC-conjugated secondary antibodies for 1 h (Zsbio, China). Afterwards, the nuclei were stained with DAPI (Zsbio, China). Images were captured using a fluorescence microscope (Olympus BX53, Tokyo, Japan).

Briefly, retinal slides were blocked with 3% H_2O_2 solution for 15 min, and then with 10% goat serum (Sigma, USA) for 30 min. Next, the retinal slices were incubated with the corresponding primary antibodies, anti-AGGF1 (1:200, Novus, NB100-455) or anti-CD31 (1:200, Proteintech, 66065-2-Ig), at 4 °C overnight. The next day, the slides

were washed and incubated with FITC- or TRITC-conjugated secondary antibodies (1:200, SIMUBIOTECH, S2003), and the nuclei were stained with DAPI (Zsbio, China). Images were captured using a fluorescence microscope (Olympus BX71, Tokyo, Japan).

Statistical analysis

Statistical analyses were performed using GraphPad Prism 8.0 software. All data were assessed blindly and are shown as the mean ± SEM. The statistical significance of differences between two experimental groups was evaluated using the 2-tailed unpaired Student's t test or one-way ANOVA with Tukey's multiple comparison test for different groups. $p < 0.05$ was considered statistically significant.

Study approval

This study was approved by the Laboratory Animal Ethical Committee Tianjin Medical University Chu Hsien-I Memorial Hospital (DXBYY-IACUC-2022065). The human study was approved by the Medical Research Ethics Committee United of the Tianjin Medical University Chu Hsien-I Memorial Hospital (Tianjin, China) (DXBYYkMEC2021-13) and the Medical Ethics Committees of Tianjin Eye Hospital (Tianjin, China) (KY-2024017) and was in accordance with the principles of the Declaration of Helsinki. Informed consent was obtained from patients for all procedures and human sample collection.

Reporting summary

Further information on research design is available in the Nature Portfolio Reporting Summary linked to this article.

Data availability

All data generated or analysed during this study are included in this article and its Supplementary Information files. All data supporting the findings described in this manuscript are available in the article and in the Supplementary Information and from the corresponding author upon request. The mass spectrometry proteomics data generated in this study have been deposited to the ProteomeXchange Consortium via the iProX partner repository with the dataset identifier PXD047004 (http://www.iprox.org/)[63,64]. Source data are provided with this paper.

References

1. Kempen, J. H. et al. The prevalence of diabetic retinopathy among adults in the United States. *Arch. Ophthalmol.* **122**, 552–563 (2004).
2. Ding, J. & Wong, T. Y. Current epidemiology of diabetic retinopathy and diabetic macular edema. *Curr. Diab Rep.* **12**, 346–354 (2012).
3. Lee, R., Wong, T. Y. & Sabanayagam, C. Epidemiology of diabetic retinopathy, diabetic macular edema and related vision loss. *Eye Vis.* **2**, 17 (2015).
4. Duh, E. J., Sun, J. K. & Stitt, A. W. Diabetic retinopathy: current understanding, mechanisms, and treatment strategies. *JCI Insight* **2**, https://doi.org/10.1172/jci.insight.93751 (2017).
5. Sapieha, P. et al. Retinopathy of prematurity: understanding ischemic retinal vasculopathies at an extreme of life. *J. Clin. Invest.* **120**, 3022–3032 (2010).
6. Hartnett, M. E. & Penn, J. S. Mechanisms and management of retinopathy of prematurity. *N. Engl. J. Med.* **367**, 2515–2526 (2012).
7. Hellström, A., Smith, L. E. H. & Dammann, O. Retinopathy of prematurity. *Lancet* **382**, 1445–1457 (2013).
8. Ben M'Barek, K., Habeler, W., Regent, F. & Monville, C. Developing Cell-Based Therapies for RPE-Associated Degenerative Eye Diseases. *Adv. Exp. Med. Biol.* **1186**, 55–97 (2019).
9. Apte, R. S. Reducing Treatment Burden in AMD. *Cell* **180**, 1033 (2020).
10. Li, J. Q. et al. Prevalence and incidence of age-related macular degeneration in Europe: a systematic review and meta-analysis. *Br. J. Ophthalmol.* **104**, 1077–1084 (2020).
11. Laforest, T. et al. Transscleral Optical Phase Imaging of the Human Retina. *Nat. Photonics* **14**, 439–445 (2020).
12. Antonetti, D. A., Klein, R. & Gardner, T. W. Diabetic retinopathy. *N. Engl. J. Med.* **366**, 1227–1239 (2012).
13. Zhang, K., Zhang, L. & Weinreb, R. N. Ophthalmic drug discovery: novel targets and mechanisms for retinal diseases and glaucoma. *Nat. Rev. Drug Discov.* **11**, 541–559 (2012).
14. Wells, J. A. et al. Aflibercept, bevacizumab, or ranibizumab for diabetic macular edema. *N. Engl. J. Med.* **372**, 1193–1203 (2015).
15. Shinkaruk, S., Bayle, M., Laïn, G. & Déléris, G. Vascular endothelial cell growth factor (VEGF), an emerging target for cancer chemotherapy. *Curr. Med. Chem. Anticancer Agents* **3**, 95–117 (2003).
16. Mintz-Hittner, H. A., Kennedy, K. A. & Chuang, A. Z. Efficacy of intravitreal bevacizumab for stage 3+ retinopathy of prematurity. *N. Engl. J. Med.* **364**, 603–615 (2011).
17. Cao, Y., Langer, R. & Ferrara, N. Targeting angiogenesis in oncology, ophthalmology and beyond. *Nat. Rev. Drug Discov.* https://doi.org/10.1038/s41573-023-00671-z (2023).
18. Grunwald, J. E. et al. Risk of geographic atrophy in the comparison of age-related macular degeneration treatments trials. *Ophthalmology* **121**, 150–161 (2014).
19. Grunwald, J. E. et al. Growth of geographic atrophy in the comparison of age-related macular degeneration treatments trials. *Ophthalmology* **122**, 809–816 (2015).
20. Rodrigues, E. B. et al. Therapeutic monoclonal antibodies in ophthalmology. *Prog. Retin Eye Res.* **28**, 117–144 (2009).
21. Tian, X.-L. et al. Identification of an angiogenic factor that when mutated causes susceptibility to Klippel-Trenaunay syndrome. *Nature* **427**, 640–645 (2004).
22. Lu, Q. et al. Angiogenic factor AGGF1 promotes therapeutic angiogenesis in a mouse limb ischemia model. *PLoS One* **7**, e46998 (2012).
23. Chen, D., Li, L., Tu, X., Yin, Z. & Wang, Q. Functional characterization of Klippel-Trenaunay syndrome gene AGGF1 identifies a novel angiogenic signaling pathway for specification of vein differentiation and angiogenesis during embryogenesis. *Hum. Mol. Genet.* **22**, 963–976 (2013).
24. Zhang, T. et al. Haploinsufficiency of Klippel-Trenaunay syndrome gene Aggf1 inhibits developmental and pathological angiogenesis by inactivating PI3K and AKT and disrupts vascular integrity by activating VE-cadherin. *Hum. Mol. Genet.* **25**, 5094–5110 (2016).
25. Wang, J. et al. Receptor and Molecular Mechanism of AGGF1 Signaling in Endothelial Cell Functions and Angiogenesis. *Arterioscler Thromb. Vasc. Biol.* **41**, 2756–2769 (2021).
26. Kihiczak, G. G., Meine, J. G., Schwartz, R. A. & Janniger, C. K. Klippel-Trenaunay syndrome: a multisystem disorder possibly resulting from a pathogenic gene for vascular and tissue overgrowth. *Int. J. Dermatol.* **45**, 883–890 (2006).
27. Wang, W. et al. Overexpression of AGGF1 is correlated with angiogenesis and poor prognosis of hepatocellular carcinoma. *Med. Oncol.* **32**, 131 (2015).
28. Zhang, X., Sun, H., Chen, W. & He, X. Elevated expression of AGGF1 predicts poor prognosis and promotes the metastasis of colorectal cancer. *BMC Cancer* **19**, 1252 (2019).
29. Stitt, A. W. AGEs and diabetic retinopathy. *Invest. Ophthalmol. Vis. Sci.* **51**, 4867–4874 (2010).
30. Durham, J. T. & Herman, I. M. Microvascular modifications in diabetic retinopathy. *Curr. Diab Rep.* **11**, 253–264 (2011).
31. Connor, K. M. et al. Quantification of oxygen-induced retinopathy in the mouse: a model of vessel loss, vessel regrowth and pathological angiogenesis. *Nat. Protoc.* **4**, 1565–1573 (2009).

32. Lee, J. et al. Angiopoietin-1 guides directional angiogenesis through integrin αvβ5 signaling for recovery of ischemic retinopathy. *Sci. Transl. Med.* **5**, 203ra127 (2013).

33. Krock, B. L., Skuli, N. & Simon, M. C. Hypoxia-induced angiogenesis: good and evil. *Genes Cancer* **2**, 1117–1133 (2011).

34. Xin, X. et al. Hypoxic retinal Muller cells promote vascular permeability by HIF-1-dependent up-regulation of angiopoietin-like 4. *Proc. Natl Acad. Sci. USA* **110**, E3425–E3434 (2013).

35. Hu, C.-J., Wang, L.-Y., Chodosh, L. A., Keith, B. & Simon, M. C. Differential roles of hypoxia-inducible factor 1alpha (HIF-1alpha) and HIF-2alpha in hypoxic gene regulation. *Mol. Cell Biol.* **23**, 9361–9374 (2003).

36. Cheung, N., Mitchell, P. & Wong, T. Y. Diabetic retinopathy. *Lancet* **376**, 124–136 (2010).

37. Yao, M.-D. et al. Role of METTL3-Dependent N6-Methyladenosine mRNA Modification in the Promotion of Angiogenesis. *Mol. Ther.* **28**, 2191–2202 (2020).

38. Chao, M.-L. et al. S-nitrosylation-mediated coupling of G-protein alpha-2 with CXCR5 induces Hippo/YAP-dependent diabetes-accelerated atherosclerosis. *Nat. Commun.* **12**, 4452 (2021).

39. Hammes, H.-P. Diabetic retinopathy: hyperglycaemia, oxidative stress and beyond. *Diabetologia* **61**, 29–38 (2018).

40. Wiley, S. R. & Winkles, J. A. TWEAK, a member of the TNF superfamily, is a multifunctional cytokine that binds the TweakR/Fn14 receptor. *Cytokine Growth Factor Rev.* **14**, 241–249 (2003).

41. Claesson-Welsh, L. & Welsh, M. VEGFA and tumour angiogenesis. *J. Intern. Med.* **273**, 114–127 (2013).

42. Witmer, A. N., Vrensen, G. F. J. M., Van Noorden, C. J. F. & Schlingemann, R. O. Vascular endothelial growth factors and angiogenesis in eye disease. *Prog. Retin. Eye Res.* **22**, 1–29 (2003).

43. Aiello, L. P. et al. Vascular endothelial growth factor in ocular fluid of patients with diabetic retinopathy and other retinal disorders. *N. Engl. J. Med.* **331**, 1480–1487 (1994).

44. Sidman, R. L. et al. The peptidomimetic Vasotide targets two retinal VEGF receptors and reduces pathological angiogenesis in murine and nonhuman primate models of retinal disease. *Sci. Transl. Med.* **7**, 309ra165 (2015).

45. Jaffe, G. J. et al. Differential Response to Anti-VEGF Regimens in Age-Related Macular Degeneration Patients with Early Persistent Retinal Fluid. *Ophthalmology* **123**, 1856–1864 (2016).

46. Rao, P. et al. Real-World Vision in Age-Related Macular Degeneration Patients Treated with Single Anti-VEGF Drug Type for 1 Year in the IRIS Registry. *Ophthalmology* **125**, 522–528 (2018).

47. Yang, S., Zhao, J. & Sun, X. Resistance to anti-VEGF therapy in neovascular age-related macular degeneration: a comprehensive review. *Drug Des. Devel. Ther.* **10**, 1857–1867 (2016).

48. Lynch, C. N. et al. TWEAK induces angiogenesis and proliferation of endothelial cells. *J. Biol. Chem.* **274**, 8455–8459 (1999).

49. Ortiz, A. et al. Considering TWEAK as a target for therapy in renal and vascular injury. *Cytokine Growth Factor Rev.* **20**, 251–258 (2009).

50. Ratajczak, W., Atkinson, S. D. & Kelly, C. The TWEAK/Fn14/CD163 axis-implications for metabolic disease. *Rev. Endocr. Metab. Disord.* **23**, 449–462 (2022).

51. Herat, L. Y., Matthews, V. B., Rakoczy, P. E., Carnagarin, R. & Schlaich, M. Focusing on Sodium Glucose Cotransporter-2 and the Sympathetic Nervous System: Potential Impact in Diabetic Retinopathy. *Int. J. Endocrinol.* **2018**, 9254126 (2018).

52. Inzucchi, S. E. et al. Retinopathy Outcomes With Empagliflozin Versus Placebo in the EMPA-REG OUTCOME Trial. *Diabetes Care* **42**, e53–e55 (2019).

53. Li, C. et al. Sodium-glucose co-transporter-2 inhibition and ocular outcomes in patients with type 2 diabetes: A systematic review and meta-analysis. *Diabetes Obes. Metab.* **23**, 252–257 (2021).

54. Gong, Q. et al. SGLT2 inhibitor-empagliflozin treatment ameliorates diabetic retinopathy manifestations and exerts protective effects associated with augmenting branched chain amino acids catabolism and transportation in db/db mice. *Biomed. Pharmacother.* **152**, 113222 (2022).

55. Herat, L. Y. et al. Determining the Role of SGLT2 Inhibition with Dapagliflozin in the Development of Diabetic Retinopathy. *Front. Biosci.* **27**, 321 (2022).

56. Herat, L. Y., Matthews, J. R., Rakoczy, E. P., Schlaich, M. P. & Matthews, V. B. Comparing and Contrasting the Effects of the SGLT Inhibitors Canagliflozin and Empagliflozin on the Progression of Retinopathy. *Front. Biosci.* **28**, 83 (2023).

57. Sabaner, M. C. et al. Do SGLT2 inhibitors prevent preclinical diabetic retinopathy? A Prospective Pilot Optical Coherence Tomography Angiography Study. *J. Fr. Ophtalmol.* **44**, 1159–1167 (2021).

58. Wollstein, G. et al. Ultrahigh-resolution optical coherence tomography in glaucoma. *Ophthalmology* **112**, 229–237 (2005).

59. Luo, Z.-W. et al. Establishment of an adult zebrafish model of retinal neurodegeneration induced by NMDA. *Int. J. Ophthalmol.* **12**, 1250–1261 (2019).

60. Wiśniewski, J. R., Zougman, A., Nagaraj, N. & Mann, M. Universal sample preparation method for proteome analysis. *Nat. Methods* **6**, 359–362 (2009).

61. Pitulescu, M. E., Schmidt, I., Benedito, R. & Adams, R. H. Inducible gene targeting in the neonatal vasculature and analysis of retinal angiogenesis in mice. *Nat. Protoc.* **5**, 1518–1534 (2010).

62. Hu, J. et al. Müller glia cells regulate Notch signaling and retinal angiogenesis via the generation of 19,20-dihydroxydocosapentaenoic acid. *J. Exp. Med.* **211**, 281–295 (2014).

63. Ma, J. et al. iProX: an integrated proteome resource. *Nucleic Acids Res.* **47**, D1211–D1217 (2019).

64. Chen, T. et al. iProX in 2021: connecting proteomics data sharing with big data. *Nucleic Acids Res.* **50**, D1522–D1527 (2022).

Acknowledgements

Author contributions

Y.C. and M.Z. designed research studies, conducted experiments, and acquired and analysed data. C.F.X., C.G.L. and S.W. assisted with bioinformatics analysis. L.S. and L.L.F. performed all human surgeries. L.M.C. and B.S. conceived the study, secured funding and supervised the work. M.Z. wrote the manuscript with support from all other authors. The order of co–first authors was decided by discussions among the 2 first authors and the corresponding author.

Competing interests

The authors declare no competing interests.

Additional information

Supplementary information The online version contains supplementary material available at https://doi.org/10.1038/s41467-025-55970-3.

Correspondence and requests for materials should be addressed to Bei Sun or Liming Chen.

Peer review information *Nature Communications* thanks Maria Grant, Rong Li and the other, anonymous, reviewer(s) for their contribution to the peer review of this work. A peer review file is available.

Reprints and permissions information is available at http://www.nature.com/reprints

Publisher's note Springer Nature remains neutral with regard to jurisdictional claims in published maps and institutional affiliations.